

A re-assessment of strong line metallicity conversions in the machine learning era.

Hossen Teimoorinia^{1,2}, Mansoureh Jalilkhany³, Jillian M. Scudder⁴, Jaclyn Jensen², Sara L. Ellison²

¹ *NRC Herzberg Astronomy and Astrophysics, 5071 West Saanich Road, Victoria, BC, V9E 2E7, Canada*

² *Department of Physics and Astronomy, University of Victoria, Victoria, BC, V8P 5C2, Canada*

³ *Department of Computer Science, University of Victoria, Victoria, BC, V8W 2Y2, Canada*

⁴ *Department of Physics and Astronomy, Oberlin College, Oberlin, Ohio, OH 44074, USA*

February 16, 2021

ABSTRACT

Strong line metallicity calibrations are widely used to determine the gas phase metallicities of individual HII regions and entire galaxies. Over a decade ago, based on the Sloan Digital Sky Survey Data Release 4 (SDSS DR4), Kewley & Ellison published the coefficients of third-order polynomials that can be used to convert between different strong line metallicity calibrations for global galaxy spectra. Here, we update the work of Kewley & Ellison in three ways. First, by using a newer data release (DR7), we approximately double the number of galaxies used in polynomial fits, providing statistically improved polynomial coefficients. Second, we include in the calibration suite five additional metallicity diagnostics that have been proposed in the last decade and were not included by Kewley & Ellison. Finally, we develop a new machine learning approach for converting between metallicity calibrations. The random forest algorithm is non-parametric and therefore more flexible than polynomial conversions, due to its ability to capture non-linear behaviour in the data. The random forest method yields the same accuracy as the (updated) polynomial conversions, but has the significant advantage that a single model can be applied over a wide range of metallicities, without the need to distinguish upper and lower branches in R_{23} calibrations. The trained random forest is made publicly available for use in the community.

Key words: galaxies: abundances — galaxies: fundamental parameters - methods: data analysis - astronomical data bases: surveys - methods: statistical

1 INTRODUCTION

The gas phase metallicity of a galaxy is a fundamental quantity that captures the cumulative history of stellar chemical enrichment, outflows and delivery of pristine material from the intergalactic medium. Commonly denoted as $12 + \log(\text{O}/\text{H})$, this metallicity is encoded into the emission line spectrum of an HII region or galaxy, and can be derived ‘directly’ by solving for the electron temperature and density. Electron densities are readily determined from nebular doublets, such as [OII] $\lambda\lambda$ 3726, 3729. In theory, electron temperatures (T_e) are similarly readily obtained, by measuring the relative strengths of emission lines of a given species that originate from different upper energy levels, e.g. [OIII] λ 5007 and the auroral line [OIII] λ 4363.

However, in practice, the weakness of the auroral lines that are used to measure T_e limits this method to metallicities below approximately $12 + \log(\text{O}/\text{H}) \sim 8.3$ for most individual spectra. The auroral line becomes weaker as metallicity increases due to the increased cooling in the interstellar medium. A common alternative

practice is therefore to use ‘strong line methods’ which use readily detectable nebular emission line ratios that have been calibrated against ‘known’ metallicities (see Kewley et al. 2019, for a review). A large variety of strong line metallicity calibrations exists in the literature, broadly falling into two categories; the so-called ‘empirical’ methods, that are calibrated against direct (T_e) metallicity measurements (e.g., Pettini & Pagel 2004; Marino et al. 2013; Curti et al. 2017) and those that are calibrated against theoretical models (e.g., McGaugh 1991; Zaritsky et al. 1994; Kewley & Dopita 2002)

Although the strong line metallicity calibrations show good internal consistency, there are strong systematic offsets between them. Therefore, attempting to combine published measurements of gas phase metallicity that have used different metallicity calibrations will result in error, with offsets as large as 0.7 dex (e.g., Kewley & Ellison 2008). In order to facilitate the combination of metallicities derived using different methods, Kewley & Ellison (2008) published an extensive assessment of the major strong line metallicity diagnostics of the time. Using metallicity data for $\sim 28,000$

galaxies in the Data Release 4 (DR4) of the Sloan Digital Sky Survey (SDSS), Kewley & Ellison (2008) published tables of coefficients for third-order polynomials that could be used to convert between any pair of diagnostics used in their study.

Although the metallicity conversions of Kewley & Ellison (2008) continue to be widely used, in the decade since their publication several advances have been made in the community. First, the samples of star-forming galaxies that can be used to calibrate metallicities has grown considerably. Secondly, several new metallicity calibrations have been introduced in the literature for which no conversions (to other diagnostics) exist. Finally, the rapid growth of machine learning technologies means that new methods exist for calibrating between different diagnostics. Such methods offer numerous advantages over the polynomial fitting approach of Kewley & Ellison (2008). For example, they can capture non-linearities in the data, make no assumptions on the form of the conversion (*viz* the third-order polynomial used in Kewley & Ellison 2008) and simplify the process by avoiding different functional forms in different regimes (e.g. upper and lower metallicity branches).

Machine learning has already gained a solid foothold in astronomical data processing. For example, neural networks and deep learning methods have been widely used for both image classification (Bottrell et al. 2019; Huertas-Company et al. 2019; Ćiprijanović et al. 2020; Ferreira et al. 2020; Teimoorinia et al. 2020a,b), ranking tasks (Teimoorinia et al. 2016; Bluck et al. 2019; Dey et al. 2019; Ellison et al. 2020), as well as for regression and pattern recognition applications (Ellison et al. 2016; Teimoorinia et al. 2017). In the realm of interstellar medium studies, neural networks and other techniques, such as random forests, have also been used to predict emission line fluxes (Teimoorinia & Ellison 2014) and metallicities from either broad band photometry (Acquaviva et al. 2015) or spectra (Ucci et al. 2018; Ho 2019).

Given the advances made since the original work of Kewley & Ellison (2008), the goal of the work presented here is three-fold. First, using a larger sample of star-forming galaxies drawn from the SDSS Data Release 7¹ (DR7; Sec.2), in Sec. 3 we re-assess the polynomial-based metallicity conversions presented by Kewley & Ellison (2008). We show that there are small systematic errors (up to ~ 0.1 dex) when the old Kewley & Ellison (2008) conversions are applied to the newer DR7 sample. New coefficients are tabulated, providing a statistically improved set of functions for researchers desiring to use polynomial based conversions between metallicity diagnostics (Sec. 3.1). Second, we extend the original suite of metallicity diagnostics with a further five calibrations that have been presented in the literature since the original work of Kewley & Ellison (2008). Finally, in Sec. 4, we develop a random forest alternative to the polynomial conversion approach. We emphasize that our goal is not to develop new metallicity calibrations, but rather to facilitate the conversion between existing methods using modern samples and methods. Our results are summarized in Sec. 5.

¹ Despite its long presence in the literature, the DR7 remains one of the most widely used galaxy datasets for spectroscopic work in the nearby universe, thanks to the public MPA/JHU database of physical properties, including emission line fluxes.

2 DATA

2.1 A brief review of Kewley & Ellison (2008)

We refer the reader to more extensive treatises on metallicity measurements in galaxies for a full pedagogical description and theoretical framework of this field (e.g., Pagel 1989; Osterbrock 1989; Stasińska 2006; López-Sánchez et al. 2012; Pérez-Montero & Amorín 2017; Kewley et al. 2019). Here, we review only the essential concepts, data selection and metallicity calibrations used in Kewley & Ellison (2008) as context for our re-assessment of that work.

Strong line metallicity diagnostics combine the fluxes from two or more nebular emission lines, which can be input into (usually, simple polynomial) functions that have been either empirically or theoretically calibrated in order to solve for the gas phase metallicity, O/H. The function that converts line fluxes to O/H are not always monotonic. One of the most well known examples of a strong line diagnostic that is double valued in O/H for a given line ratio, is the family of R_{23} diagnostics, where

$$R_{23} = \frac{[OII]\lambda 3727 + [OIII]\lambda 4959 + [OIII]\lambda 5007}{H\beta} \quad (1)$$

Additional constraints are required to break the R_{23} degeneracy in order to determine whether the galaxy (or HII region) lies on the upper or lower branch of the calibration. Kewley & Ellison (2008) use the ratio of [NII]/[OII] to break the R_{23} degeneracy, since this ratio is not sensitive to ionization parameter and largely monotonic with metallicity in the range of SDSS galaxy metallicities. Whilst this approach can work well for metal-rich and metal-poor galaxies, at intermediate metallicities the calibration can be ambiguous and O/H is more uncertain.

Kewley & Ellison (2008) select their galaxy sample from the SDSS DR4. A S/N of at least 8 is required in the [OII], [OIII], [NII], [SII] and Balmer lines used in the metallicity calibrations. *g*-band fibre covering fractions are required to be at least 20 per cent, enforcing an effective lower redshift cut $z \sim 0.04$. An upper redshift cut of $z < 0.1$ is also imposed. Galaxies dominated by active galactic nucleus (AGN) emission are removed using the criteria presented in Kewley et al. (2006). The resulting sample contains $\sim 28,000$ star-forming galaxies. Emission line fluxes were corrected by measuring the Balmer decrement and applying the Milky Way extinction curve of Cardelli et al. (1989).

Kewley & Ellison (2008) considered 10 different metallicity calibrations: the direct (or T_e) method and nine different strong line methods. T_e based metallicities are not available for the majority of individual SDSS galaxies, hence we consider it no further here (but see (Andrews & Martini 2013; Curti et al. 2017) for works that have derived T_e based metallicities for SDSS spectral stacks). Of the nine strong line methods, we exclude two from our current work. First, we exclude the calibration of Denicoló et al. (2002); this calibration is based on the ratio of [NII]/ $H\alpha$ and has been superseded by several other calibrations used in this work. Second, we also exclude Pilyugin & Thuan (2005); as shown by Kewley & Ellison (2008) this diagnostic does not cross-calibrate well with other methods.

Below we briefly review the remaining seven strong line methods used by Kewley & Ellison (2008) that we will re-calibrate in the work presented here:

- McGaugh (1991). Hereafter M91, this calibration uses R_{23} and is calibrated using theoretical models. Kewley & Ellison (2008) calibrate the upper and lower branches of this diagnostic with

separate polynomial fits, whose degeneracy is broken with the $[\text{NII}]/[\text{OII}]$ ratio.

- Zaritsky et al. (1994). Hereafter Z94, this is an average of three previously published theoretically calibrated R_{23} diagnostics and is applicable only to the upper branch.

- Kewley & Dopita (2002). Hereafter KD02, this diagnostic is theoretically calibrated. KD02 is applied in two regimes - at high metallicities the calibration is based on the ratio $[\text{NII}]/[\text{OII}]$, and at low metallicities it uses an average of several R_{23} methods.

- Kobulnicky & Kewley (2004). Hereafter KK04, this calibration uses the same theoretical grids as KD02. Application of the KK04 calibration is a multi-step process that entails an assessment of whether the galaxy is on the upper or lower R_{23} branch, following an initial estimate of the ionization parameter from the ratio of $[\text{OIII}]/[\text{OII}]$. The final metallicity and ionization parameter is determined through an iterative process based on R_{23} .

- Pettini & Pagel (2004) N2 and O3N2. Hereafter PP04 N2 and PP04 O3N2, these diagnostics are both empirically² calibrated against direct (T_e) metallicities, and use either the ratio of $[\text{NII}]/\text{H}\alpha$ (PP04 N2) or additionally including $[\text{OIII}]/\text{H}\alpha$ (PP04 O3N2). Specifically, the following indices are defined:

$$\text{N2} = \log\left(\frac{[\text{NII}]\lambda 6583}{\text{H}\alpha}\right) \quad (2)$$

and

$$\text{O3N2} = \log\left(\frac{[\text{OIII}]\lambda 5007/\text{H}\beta}{[\text{NII}]\lambda 6583/\text{H}\alpha}\right) \quad (3)$$

The advantage of both of N2 and O3N2 calibrations is that they are single valued and do not require dust correction of the emission line fluxes, because the lines used in the ratios are close in wavelength. However, PP04 N2 (as with any N2 based calibration) has the limitation that it tends to saturate at higher metallicities.

- Tremonti et al. (2004). Hereafter T04, this calibration uses a broader suite of emission lines, including $[\text{NII}]$ and $[\text{SII}]$ in addition to the commonly used oxygen and Balmer lines. Unlike the other calibrations used by Kewley & Ellison (2008), T04 derive metallicities from a statistical assessment of a large suite of spectral synthesis models. The T04 metallicities are therefore not computed by us (nor were they by Kewley & Ellison 2008) from the raw emission line fluxes, but rather are taken directly from the MPA/JHU catalog. We note that the large number of galaxies with available T04 metallicities, despite the large number of lines required, is because of the specific S/N requirements adopted in that work (which are not applied to all of the listed lines).

2.2 New calibrations considered in this paper

We include five new metallicity calibrations in the current study that were not available to Kewley & Ellison (2008), but have become widely used in the literature since their publication. We review here their main properties, for comparison with the diagnostics used in Kewley & Ellison (2008), but refer the reader to the original papers for full details.

- Marino et al. (2013) N2 and O3N2. Hereafter M13 N2 and M13 O3N2, this study compiled over 600 HII regions with T_e based metallicities. Two strong line diagnostics were calibrated

based upon this large sample, $[\text{NII}]/\text{H}\alpha$ (i.e. the N2 index) and $([\text{OIII}]/\text{H}\beta)/([\text{NII}]/\text{H}\alpha)$ (i.e. the O3N2 index). As with other N2 diagnostics, saturation is a problem at higher metallicities, whereas O3N2 can be used up to $12 + \log(\text{O}/\text{H}) \sim 8.9$.

- Dopita et al. (2016). Hereafter D16, this diagnostic uses a unique set of emission lines amongst those studied here. By combining $[\text{NII}]$, $\text{H}\alpha$ and $[\text{SII}]$, which are all located close together in wavelength space, this metallicity diagnostic offers several advantages. First, it is independent of extinction. Second, all of the emission lines can be covered in one spectral setting, even if the instrumental coverage is relatively narrow. Finally, this diagnostic is characterised by a linear function up to super-solar metallicities ($12 + \log(\text{O}/\text{H}) \approx 9.05$) and is largely independent of ionization parameter.

- Curti et al. (2017) N2 and O3N2. Hereafter C17 N2 and C17 O3N2, this study used over 110,000 star-forming galaxies drawn from the SDSS DR7 (the same dataset from which we will draw our sample) to derive an empirical metallicity calibration over an unprecedentedly broad range in O/H by stacking galaxies in narrow bins of $[\text{OII}]$ and $[\text{OIII}]$ relative to $\text{H}\beta$. The very high S/N ratios achieved in the stacking process enable a detection of $[\text{OIII}] \lambda 4363$, which is required to determine the electron temperature and thereby solve for metallicity. As with Marino et al. (2013), Curti et al. (2017) calibrated their T_e based metallicities for two strong line ratios, N2 and O3N2.

Table 1 summarizes the 12 diagnostics used in this paper; seven from the original Kewley & Ellison (2008) work and five new ones. Table 1 also summarizes the metallicity regime over which the calibrations are valid and the emission lines used.

2.3 SDSS DR7 Galaxy Selection

Emission line fluxes used in this work are taken from the publicly available SDSS DR7 MPA/JHU catalog³, e.g. Brinchmann et al. (2004). The emission lines in this catalog have been corrected for underlying stellar absorption and for Galactic extinction. We further correct for internal extinction by assuming an intrinsic $\text{H}\alpha/\text{H}\beta=2.85$ and a Small Magellanic Cloud extinction curve (Pei 1992)⁴.

We begin by selecting all galaxies from the DR7 that are classified as star-forming according to the Kauffmann et al. (2003) definition. For this selection, we require that the S/N in the four emission lines required for the star-forming classification have a $\text{S/N} > 3$. Approximately 159,000 galaxies are thus selected.

In order to identify galaxies for which robust, global metallicities may be estimated, further cuts are required on emission line S/N and fibre covering fraction. In order to facilitate an equitable comparison with the conversions of Kewley & Ellison (2008), we adopt the same criteria as in that work, i.e., g-band fibre covering fraction of at least 20 per cent, an upper redshift cut of 0.1 and a minimum S/N in the emission lines required for a given calibration of 8. The application of the first two of these criteria result in a sample that is reduced from $\sim 159,000$ to $\sim 61,000$. The S/N requirement further reduces the sample to a size that depends on the specific set of emission lines required for a given calibration. The final column of Table 1 summarizes the number of galaxies selected for each calibration. The number of galaxies used in each pairwise

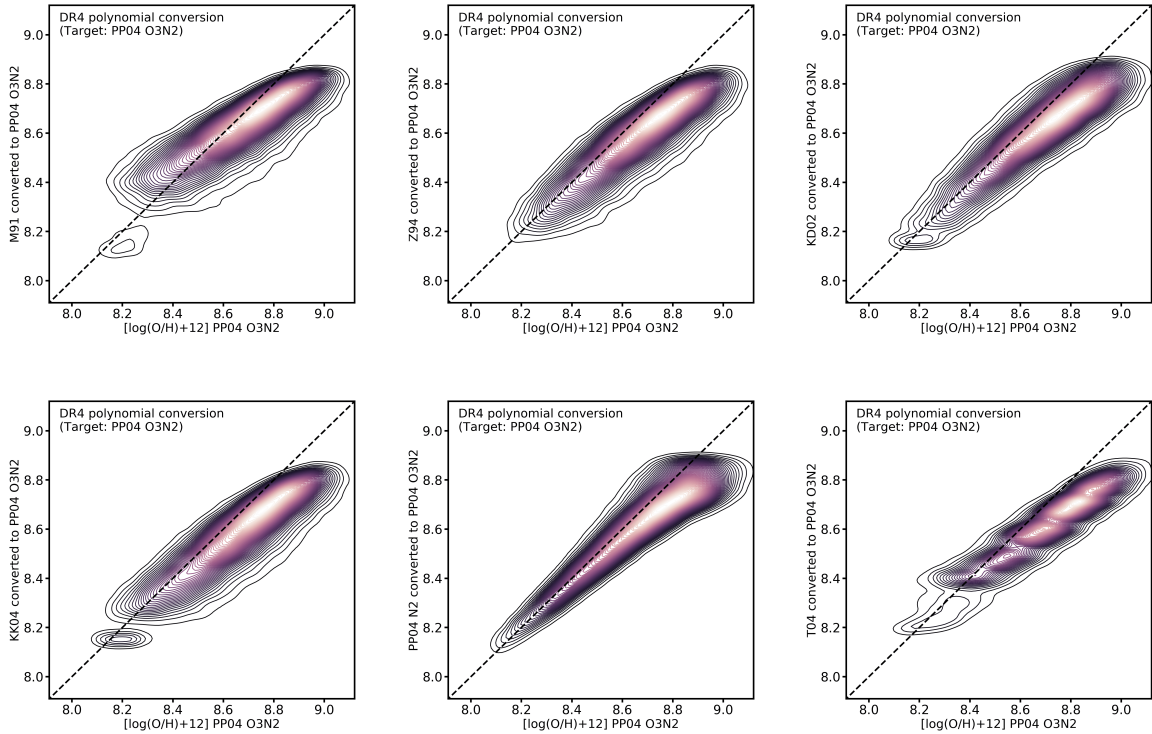
² A small number (6/137) of the HII regions used in the Pettini & Pagel (2004) diagnostic are calibrated using theoretical models. Given the vast majority of T_e based metallicities used by PP04, we refer to this as an empirical method.

³ <https://wwwmpa.mpa-garching.mpg.de/SDSS/>

⁴ We test the influence of choosing a Milky Way type extinction curve and find that it has negligible impact on the calculated metallicities.

Table 1. The list of metallicity calibrations used in this paper and number of galaxies in the DR7 dataset.

Metallicity	Reference	Range of validity	Lines required	N galaxies
M91	McGaugh (1991)	$7.24 < 12 + \log(\text{O}/\text{H}) < 9.4$	[NII] λ 6583, [OII] λ 3727, [OIII] λ 5007, H β	32275
Z94	Zaritsky et al. (1994)	$12 + \log(\text{O}/\text{H}) > 8.35$	[NII] λ 6583, [OII] λ 3727, [OIII] λ 5007, H β	31701
KD02	Kewley & Dopita (2002)	$8.2 < 12 + \log(\text{O}/\text{H}) < 9.4$	[NII] λ 6583, [OII] λ 3727, [OIII] λ 5007, H β	37899
KK04	Kobulnicky & Kewley (2004)	$7.6 < 12 + \log(\text{O}/\text{H}) < 9.2$	[NII] λ 6583, [OII] λ 3727, [OIII] λ 5007, H β	32168
PP04 N2	Pettini & Pagel (2004)	$-2.5 < \text{N}2 < -0.3$	[NII] λ 6583, H α	44726
PP04 O3N2	Pettini & Pagel (2004)	$\text{O}3\text{N}2 < 2.0$	[OIII] λ 5007, H β , H α , [NII] λ 6583	44590
T04	Tremonti et al. (2004)	N/A	[NII] λ 6583, [OII] λ 3727, [OIII] λ 5007, [OI] HeI, H β , H α , [SII] λ 6717, 6731	50774
M13 N2	Marino et al. (2013)	$-1.6 < \text{N}2 < -0.2$	[NII] λ 6583, H α	45036
M13 O3N2	Marino et al. (2013)	$-1.1 < \text{O}3\text{N}2 < 1.7$	[OIII] λ 5007, H β , H α , [NII] λ 6583	44085
D16	Dopita et al. (2016)	$7.76 < 12 + \log(\text{O}/\text{H}) < 9.05$	[NII] λ 6583, H α , [SII] λ 6717, 6731	42892
C17 N2	Curti et al. (2016)	$7.6 < 12 + \log(\text{O}/\text{H}) < 8.85$	[NII] λ 6583, H α	43743
C17 O3N2	Curti et al. (2016)	$7.6 < 12 + \log(\text{O}/\text{H}) < 8.85$	[OIII] λ 5007, H β , H α , [NII] λ 6583	44946

**Figure 1.** Assessment of the DR4-derived metallicity conversions on the expanded DR7 dataset. In each panel, the DR7-derived PP04 O3N2 metallicity is shown on the x-axis. For the six other strong line methods calibrations with conversions by Kewley & Ellison (2008) that are used in this paper, the y-axis shows each metallicity diagnostic converted to PP04 O3N2 using the original DR4 polynomial coefficients. The deviations of the data from the diagonal 1:1 dashed line demonstrate that the DR4 conversions are not optimized for the DR7 dataset.

cross-calibration (which requires a $S/N > 8$ in the lines used for both calibrations in a given conversion) is further given in Tables A1 - A12.

3 THE POLYNOMIAL CONVERSION METHOD

Derived from a sample of $\sim 28,000$ star-forming galaxies from the SDSS DR4, Kewley & Ellison (2008) presented tabulated coefficients for a third order polynomial that could be used to convert between different metallicity calibrations. We begin by re-assessing

the validity of these metallicity conversions as applied to our larger DR7 dataset. We will then extend these polynomial based conversions to include the five additional diagnostics summarized in Section 2.2.

3.1 A re-assessment of Kewley & Ellison (2008) conversions using SDSS DR7 data

Of the ten original metallicity diagnostics explored in Kewley & Ellison (2008), conversions between eight of the strong line metallicity calibrations were presented in Kewley & Ellison (2008). Of

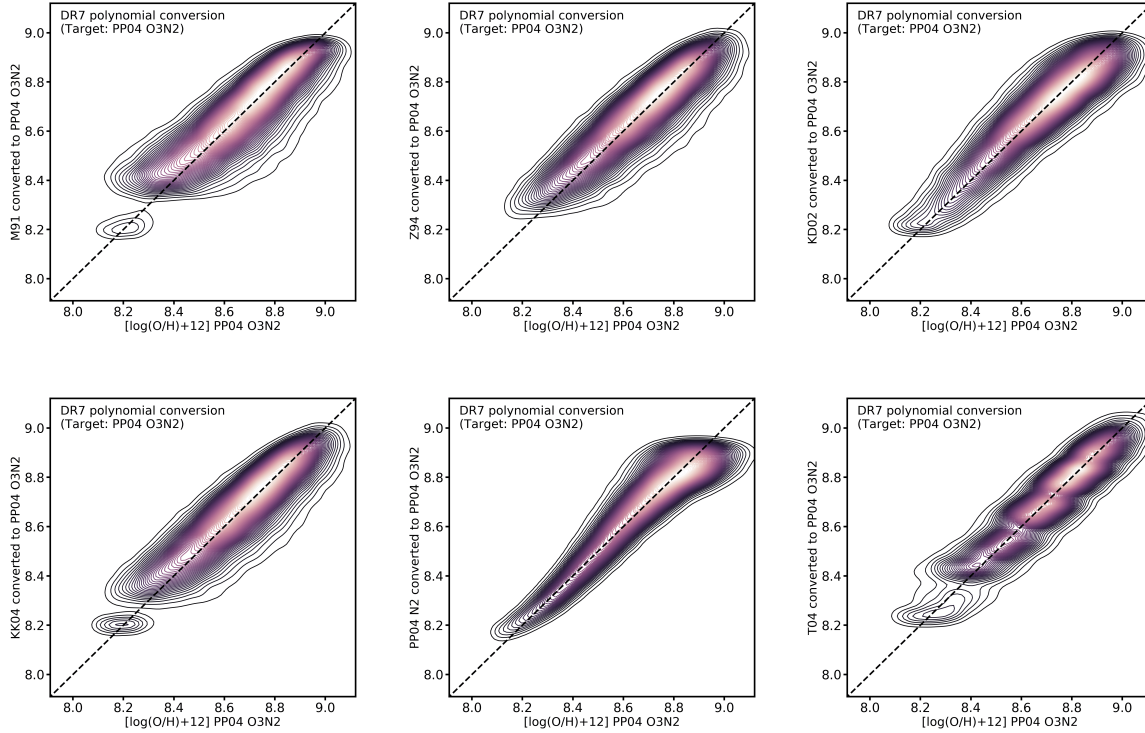


Figure 2. The same plot as Fig 1, but with the newly determined polynomial coefficients derived from the DR7 dataset. The systematic offsets found in Fig 1 using the DR4 coefficients have now been removed and the converted metallicities perform well.

these eight, we have removed Denicolo et al. (2002), for the reasons described in Sec. 2.1, leaving the following seven strong line diagnostics: M91, Z94, KD02, KK04, PP04 N2, PP04 O3N2 and T04. Gas phase metallicities are computed for the first six of these diagnostics (the T04 metallicity is taken directly from the MPA/JHU catalog) for our DR7 sample of galaxies (see the last column of Table 1 for the number of galaxies available for each diagnostic).

Fig. 1 shows some examples of the Kewley & Ellison (2008) conversion coefficients (derived for DR4) as applied to our DR7 dataset. For this exemplar, we have selected the PP04 O3N2 as the target diagnostic, which is shown on the x-axis of each panel of Fig. 1 for the DR7 dataset. Each of the other six diagnostics is then converted onto the PP04 O3N2 system using the polynomial coefficients derived by Kewley & Ellison (2008). If the conversions worked perfectly, then the converted version of a given calibration (y-axis) should be identical to its directly measured value (x-axis), and the points will line up along the diagonal 1:1 dashed line.

The results shown in Fig. 1 (and a thorough assessment of all the combinations of targets and conversions, not shown here for brevity) confirm that the Kewley & Ellison (2008) DR4-derived coefficients are not optimized for the DR7 dataset. The offsets between the converted and target metallicities are typically quite small, < 0.1 dex, but the large dataset shows that these effects are statistically significant, and depending on the calibration in question, can affect a significant fraction of galaxies.

We determine that the origin of these offsets and biases is likely due to changes in the emission line flux values, which are typically higher in the DR7 than in the DR4. While uniform enhancements in the line fluxes should not produce systematic biases in metallicity values, we find that not all emission lines are stronger

in the DR7 by the same percentage, which will present a bias when comparing metallicities based on different emission line ratios. Fig. 1 shows conversions between calibrations which use different emission line ratios, and are therefore strongly affected by this change in line strengths. Conversions between calibrations based on the same emission lines are less discrepant between the two data sets.

We therefore re-compute improved coefficients between the seven metallicity diagnostics in common between our sample and that of Kewley & Ellison (2008), using an identical functional form of a third order polynomial. The new coefficients are tabulated in Tables A1 – A7. Fig. 2 shows the same combination of conversions as Fig. 1, but using these updated polynomial coefficients. The systematic offsets and biases that were present in Fig. 1 have now been largely eliminated.

3.2 Polynomial coefficients for converting five additional diagnostics

In addition to the diagnostics previously presented in Kewley & Ellison (2008), we have additionally derived conversions, using the polynomial method, for the five additional diagnostics summarized in Sec 2.2 (M13 N2, M13 O3N2, D16, C17 N2 and C17 O3N2). We again use a third-order polynomial, in order to be consistent with the other diagnostic conversions. The coefficients for these new diagnostic conversions are presented in Tables A8 – A12.

In Fig. 3, we show an example of these new conversions, using C17 O3N2 as the target metallicity diagnostic. Similar to Figs 1 and 2, the C17 O3N2 metallicities (derived directly from the SDSS DR7 spectra) in a given calibration are plotted on the x-axis, with each of the other diagnostics, converted into C17 O3N2 via their poly-

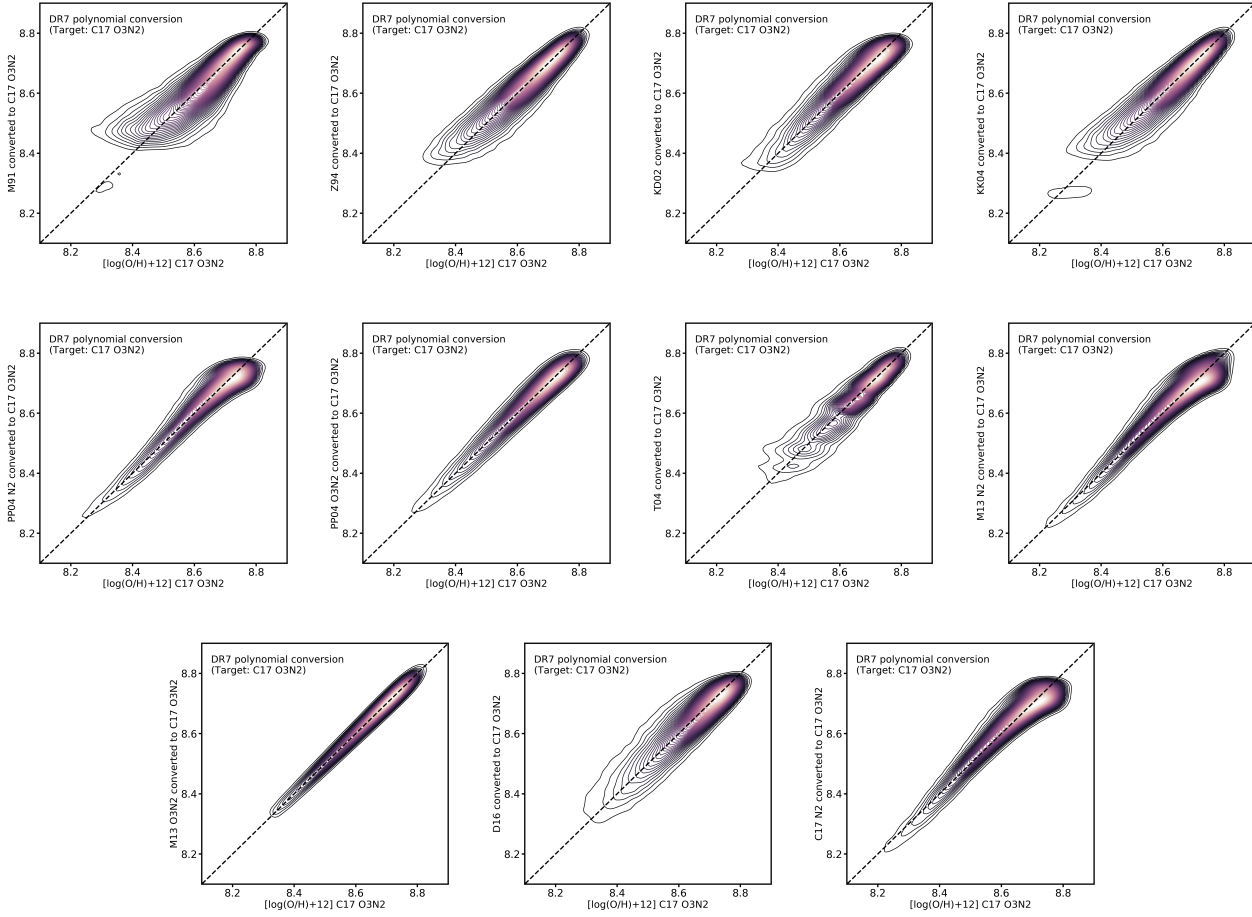


Figure 3. Metallicity conversions using the polynomial method and DR7 data for an expanded set of diagnostics. In this example, C17 O3N2 is the target metallicity diagnostic and the other 11 calibrations have been converted to it using the coefficients in the Appendix tables.

nomial fit, are plotted on the y-axis. The new conversions show no systematic offsets or skewed behaviour, confirming that the third-order polynomial fit between pairs of calibrations is a good representation of the data.

Taken together, the updated coefficients in Tables A1 – A12 represent an improvement in both accuracy and available diagnostics over the original work on this topic by Kewley & Ellison (2008). Given the cumbersome nature of the table format, we have also developed a Graphical User Interface (GUI) into which these coefficients are coded, to facilitate the use of the polynomial functions within the community. We note for transparency that the metallicities output by this GUI are rounded to three decimal places. The GUI can be downloaded here: [Polynomial-link](#).

4 THE RANDOM FOREST METHOD

Figures 2 and 3 show that, for the 12 strong line metallicity calibrations presented here, a third-order polynomial can be used to convert between diagnostics with no systematic offsets. None the less, there are several reasons to motivate an investigation of non-linear solutions to these conversions. First, since a polynomial function is a linear model based on coefficients, it is less able to capture any nonlinear features in the correlations between calibrations than a random forest model which is nonlinear by construction. A further

potential advantage of a machine learning approach is that degeneracy breaking decisions (such as upper and lower branch of R_{23}) are naturally included in the model (see also the discussion in Ucci et al. 2018; Ho et al. 2019).

4.1 Methodology

A random forest (RF) is a supervised and non-parametric model used for regression and classification problems. In a non-parametric model, there is no internal parameter to train and learn. Since an RF is a supervised method, it implies that for a vector of input parameters, there is a target vector that we want to predict. An RF consists of several similar decision trees - the building blocks of the random forest model. A decision tree is a system of yes/no options (see Fig.4 for a schematic of the process). This system is a recursive partitioning model in which, from the root node, the input data is repeatedly divided and sub-divided. First, the root node is split into two (internal) nodes based on the binary decisions on an input value of the data under study. Then the procedure is repeated for the two nodes (i.e., in layer-2). In this way, the depth can be increased. The depth of a tree is a parameter that is chosen by the user. We can stop the tree from growing according to some criteria such as the maximum depth or the minimum samples in a node. The end result is a decision tree with final nodes that are called leaves. Each

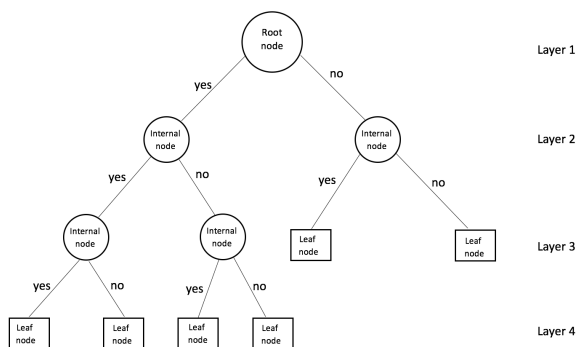


Figure 4. A schematic diagram of the structure of a decision tree. A random forest is comprised of many individual decision trees, which mitigates the problem of over-fitting the data.

leaf consists of a set of arranged input parameters and the corresponding target value. In a regression problem, the average value of the targets in a leaf will be predicted in that leaf. A single tree has the potential for overfitting as we increase the depth of the tree. To tackle this problem, we can extend the use of a single decision tree to a ‘forest’ (Tin Kam Ho 1998).

In a RF model, a set (e.g., 100) of similar trees are made (i.e., with the same depth and the same decision procedure). Input to the first tree is a portion (e.g., 20%) of the primary input data, which is randomly selected (with replacement) and then fed to the tree. This procedure is repeated for all trees one by one. In this way, each tree’s prediction will be a slightly different from other trees due to the randomization procedure. The final regression prediction is the average of all predicted results of all similar trees. This method prevents overfitting and generally gives better and more accurate results. One advantage of using an RF model is that for a two-branch problem, such as R_{23} metallicity conversions in Kewley & Ellison (2008), one single RF model can predict the metallicity values in branches, without the need for a user-defined break point between the branches. An RF approach therefore not only reduces the number of required models, but also removes the need for subjective boundaries. In this work, we use the RF package from scikit-learn (Pedregosa et al. 2011). We use an RF with 100 estimators (trees) and increase the depth of the trees to have at least 10 members (metallicities) in leaves, which is found to be the optimal number for the present work.

4.2 Results from the random forest

Fig. 5 has the same format as Fig. 3, i.e. using C17 O3N2 as the target and converting from the 11 other strong line methods. Fig. 5 shows that the RF models have successfully converted from the base to the target metallicity diagnostic with no systematic offsets or skewness.

Visually, Figs. 5 (RF conversions with C17 O3N2 as the target) and 2 (DR7 polynomial fits with C17 O3N2 as the target) look very similar. In Fig. 6 we compare the two methods quantitatively by plotting the scatter within our new polynomial (blue circles) and random forest (red squares) conversions. In this example, C17 O3N2 is again the target metallicity and the scatter is shown for each of the other 11 metallicity calibrations used in the conversion. From Fig. 6, it can be seen that for any given base calibration, when converting to the C17 O3N2 calibration, the scatter for the two techniques is almost identical. We have found this to be generally true for any combination of metallicity diagnostics, indicating

that in terms of overall performance, the polynomial and RF methods are equally strong. Therefore, the random forest approach does not offer any performance advantage over the polynomial method⁵. However, operationally, the random forest is simpler for the user, requiring no subjective assessment of degeneracies or iterative solution for ionization parameter. We caution that this RF model has been trained and tested on the DR7 data set only, and may not transfer well to other data sets.

In order to facilitate the application of our RF model within the community, we have developed a GUI for all metallicity conversions in this paper. The interface uses 132 different RF models for the conversions. As with the polynomial GUI, the metallicities output by this RF GUI are rounded to 3 decimal places. The code can be downloaded from (RF-link) and uses the same format as the polynomial GUI also provided as a companion to this paper.

Kewley & Ellison (2008) demonstrated (their Fig. 2) that the mass-metallicity relation shows a range of 0.7 dex in metallicity (at fixed stellar mass) for the suite of calibrations used in that paper. Kewley & Ellison (2008) also demonstrated (their Fig. 4) that after the application of their metallicity conversions, these variations were effectively removed. In Fig. 7 and Fig. 8 we repeat this demonstration with the full suite of 12 calibrations used in this paper and the application of the random forest conversions. In Fig. 7, we show a third order polynomial fit to the mass-metallicity relation for the 12 calibrations in the original metallicity sample, prior to any conversions, described in Table 1. The stellar masses come from the MPA-JHU data release of Brinchmann et al. (2004). Broadly consistent with the results of Kewley & Ellison (2008), we find a 0.6 dex range in metallicity between calibrations at fixed stellar mass. This is slightly less than the range found by Kewley & Ellison (2008) because we have excluded the most deviant calibration (Pilyugin & Thuan 2005) from our suite. In Fig. 8, we show the improvement to the mass-metallicity relation for the DR7 sample after the application of the RF metallicity conversions. In each of the 12 panels, one of the metallicity calibrations is selected in turn as the target. The other 11 diagnostics are then converted to this target using our RF model. For each of the 12 metallicity calibrations, it can be seen that after the RF conversion has been applied, the mass-metallicity relation is invariant to the choice of metallicity diagnostic.

5 SUMMARY

We have presented a three step re-assessment of the metallicity calibration conversions originally presented in Kewley & Ellison (2008). First, we have approximately doubled the number of star-forming galaxies in the sample, by extending the original DR4 sample used by Kewley & Ellison (2008) to the DR7. Our complete star-forming galaxy sample, with cuts on covering fraction and redshift, contains $\sim 61,000$ galaxies and the samples for the individual metallicity calibrations (which have further cuts on emission line S/N) typically contain $\sim 40,000$ galaxies. Seven of the strong line metallicity calibrations presented in Kewley & Ellison (2008) are considered in this work. We find that the metallicity conversions derived by Kewley & Ellison (2008) are not optimized for use on the DR7 dataset (Fig. 1). The second stage of our analysis

⁵ Because of the discrete nature of the RF ‘leaf’, there may be more clustering around particular target metallicities in the RF model, compared to the polynomial conversion. The preservation of equal magnitudes of scatter indicates that this is not causing major biases in the conversion process.

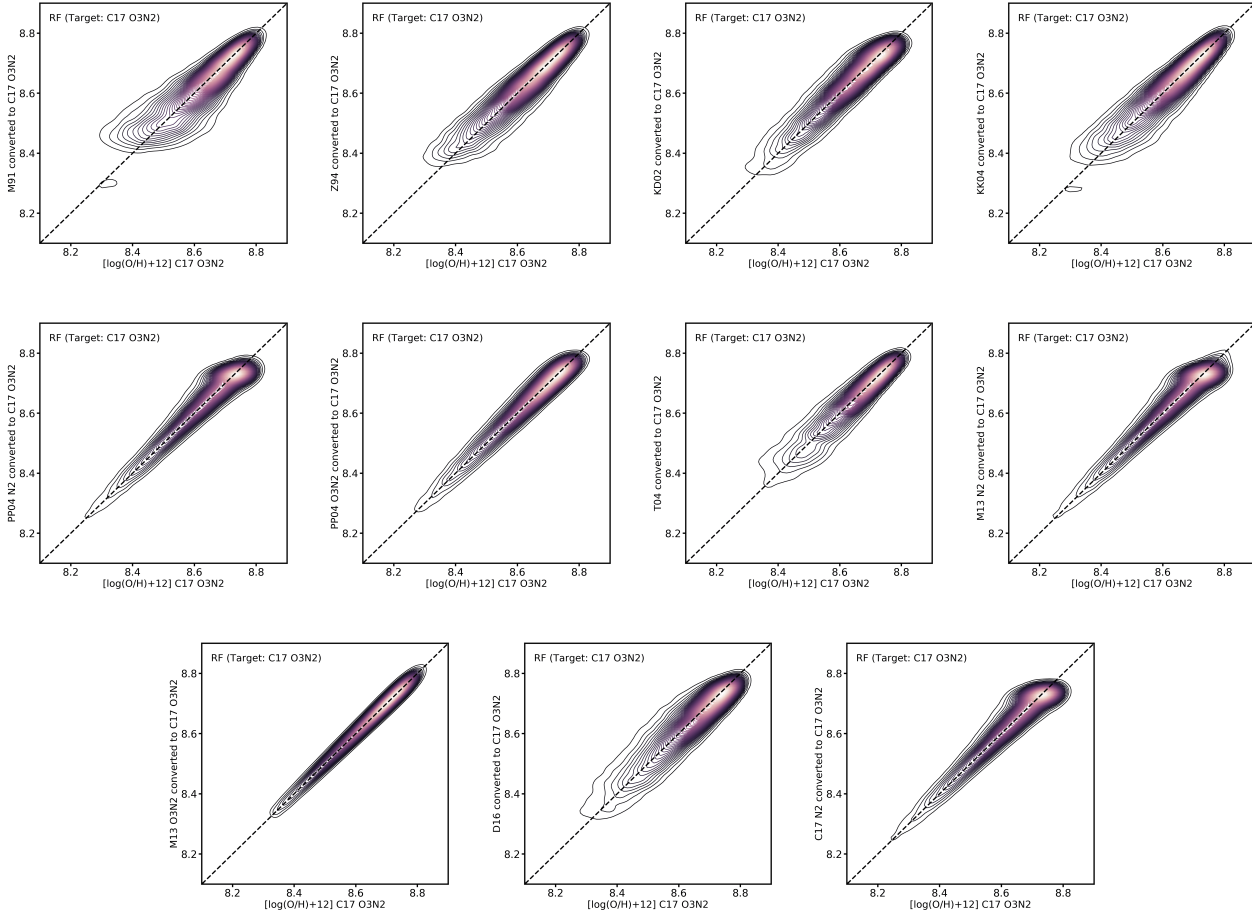


Figure 5. The same as Fig. 3 but using a random forest method for calculating the metallicity conversions.

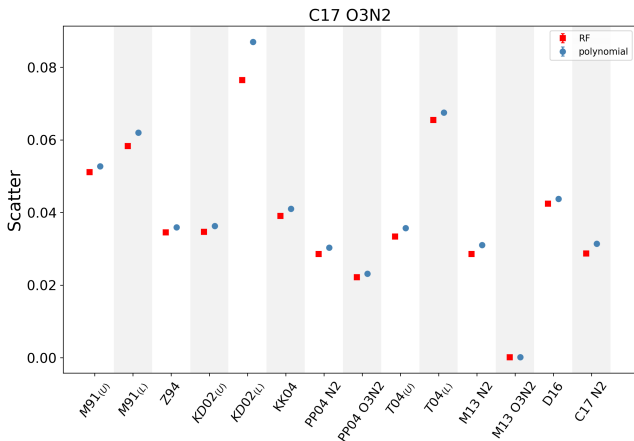


Figure 6. A comparison between the scatter obtained by the new polynomial equations and the RF results. The results do not show a significant difference. The title shows the base, and on the ‘x’ axis the input is shown.

is therefore to repeat the third order polynomial fitting procedure used by Kewley & Ellison (2008) to derive new coefficients (Tables A1 - A7) which better represent the DR7 data (Fig. 2). We also derive coefficients for five additional strong line metallicity diagnostics that have been presented in the literature since the original

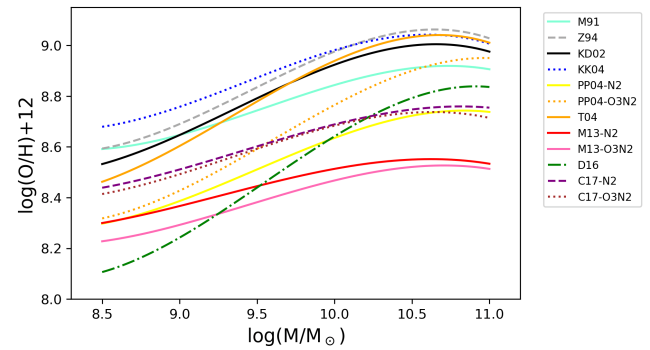


Figure 7. Third order polynomial fits to the mass-metallicity relations for the original metallicity sample as recalculated for the DR7, for each of the 12 calibrations, described in Table 1.

work of Kewley & Ellison (2008) (Fig. 3 and Tables A8 - A12). Taken together, the coefficients presented in Table A1 - A12 represent the most complete polynomial based conversion factors for global galaxy metallicities.

The third stage of our re-assessment of metallicity conversions focuses on the potential improvement over polynomial fits that machine learning methods may provide. Such methods can potentially better capture complexity in the data, and have the specific advan-

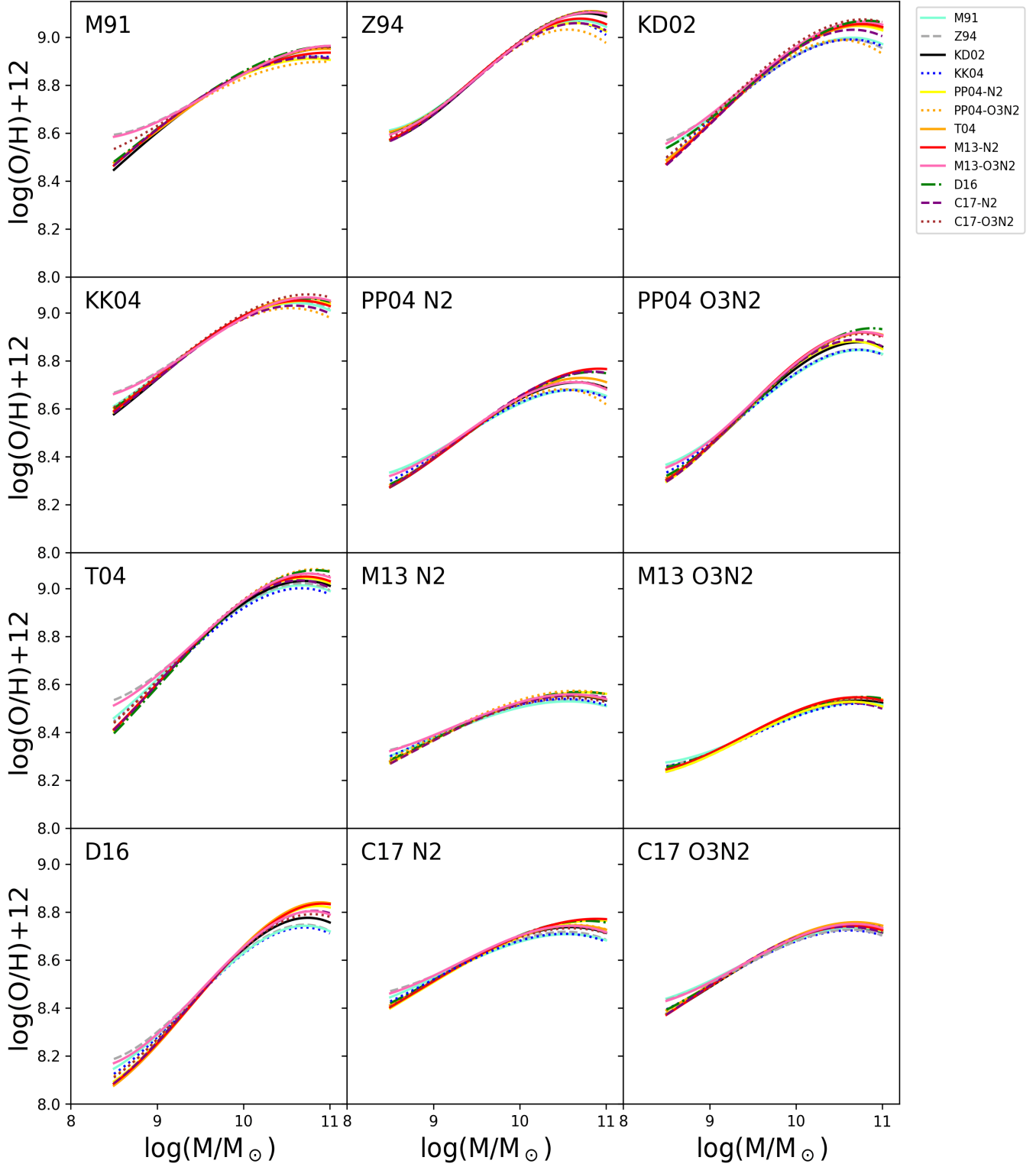


Figure 8. The mass-metallicity relations derived from the DR7 data after application of the random forest conversions. In each panel, one of the 12 metallicity calibrations is selected as the target (top left legend) and the other 11 diagnostics are converted to this target. The curves are all in excellent agreement, showing that the conversions have successfully re-calibrated each diagnostic to a common scale.

tage in the realm of metallicity determinations of not requiring separate functions for upper and lower branch R_{23} calibrations. We successfully model the metallicity conversions between each of the 12 diagnostics presented in this work (Fig 5). Despite the additional potential of the random forest compared to a simple third order polynomial fit, the two methods perform very similarly. The predicted metallicity conversions are very similar (e.g. comparing Fig. 3 and Fig. 5) and the uncertainties of the two methods are almost identical (Fig. 6). Nonetheless, the RF offers the afore-mentioned advantage of avoiding uncertainty in decisions concerning upper and lower branch R_{23} branches, and therefore may be more robust for metallicities in the turnover regime at intermediate metallicities. We have made our random forest models publicly available in a user-friendly format for use by the community.

ACKNOWLEDGEMENTS

SLE gratefully acknowledges the receipt of an NSERC Discovery Grant.

We are grateful to the MPA/JHU groups for making their SDSS catalogs public. The work presented here would not have been possible without this resource.

Funding for the SDSS and SDSS-II has been provided by the Alfred P. Sloan Foundation, the Participating Institutions, the National Science Foundation, the U.S. Department of Energy, the National Aeronautics and Space Administration, the Japanese Monbukagakusho, the Max Planck Society, and the Higher Education Funding Council for England. The SDSS Web Site is <http://www.sdss.org/>.

The SDSS is managed by the Astrophysical Research Consortium for the Participating Institutions. The Participating Institutions are the American Museum of Natural History, Astrophysical Institute Potsdam, University of Basel, University of Cambridge, Case Western Reserve University, University of Chicago, Drexel University, Fermilab, the Institute for Advanced Study, the Japan Participation Group, Johns Hopkins University, the Joint Institute for Nuclear Astrophysics, the Kavli Institute for Particle Astrophysics and Cosmology, the Korean Scientist Group, the Chinese Academy of Sciences (LAMOST), Los Alamos National Laboratory, the Max-Planck-Institute for Astronomy (MPIA), the Max-Planck-Institute for Astrophysics (MPA), New Mexico State University, Ohio State University, University of Pittsburgh, University of Portsmouth, Princeton University, the United States Naval Observatory, and the University of Washington.

6 DATA AVAILABILITY

We have developed two GUIs for all polynomial and RF metallicity conversions in this paper. Each interface uses 132 different set of coefficients and models for the conversions. The data underlying this article are available in:

Polynomial: (Polynomial-link).

Random Forest: (RF-link)

References

- Acquaviva V., Raichoor A., Gawiser E., 2015, *ApJ*, 804, 1, 8
 Andrews B. H., Martini P., 2013, *ApJ*, 765, 2, 140
 Bluck A. F. L., Bottrell C., Teimoorinia H., et al., 2019, *MNRAS*, 485, 1, 666
 Bottrell C., Hani M. H., Teimoorinia H., et al., 2019, *MNRAS*, 490, 4, 5390
 Brinchmann J., Charlot S., White S. D. M., et al., 2004, *MNRAS*, 351, 4, 1151
 Cardelli J. A., Clayton G. C., Mathis J. S., 1989, *ApJ*, 345, 245
 Čiprijanović A., Snyder G. F., Nord B., Peek J. E. G., 2020, *Astronomy and Computing*, 32, 100390
 Curti M., Cresci G., Mannucci F., Marconi A., Maiolino R., Esposito S., 2017, *MNRAS*, 465, 2, 1384
 Denicoló G., Terlevich R., Terlevich E., 2002, in *Revista Mexicana de Astronomía y Astrofísica Conference Series*, edited by W. J. Henney, J. Franco, M. Martos, vol. 12 of *Revista Mexicana de Astronomía y Astrofísica Conference Series*, 257–257
 Dey B., Rosolowsky E., Cao Y., et al., 2019, *MNRAS*, 488, 2, 1926
 Dopita M. A., Kewley L. J., Sutherland R. S., Nicholls D. C., 2016, *Ap&SS*, 361, 61
 Ellison S. L., Teimoorinia H., Rosario D. J., Mendel J. T., 2016, *MNRAS*, 455, 1, 370
 Ellison S. L., Thorp M. D., Lin L., et al., 2020, *MNRAS*, 493, 1, L39
 Ferreira L., Conselice C. J., Duncan K., Cheng T.-Y., Griffiths A., Whitney A., 2020, *ApJ*, 895, 2, 115
 Ho I. T., 2019, *MNRAS*, 485, 3, 3569
 Huertas-Company M., Rodriguez-Gomez V., Nelson D., et al., 2019, *MNRAS*, 489, 2, 1859
 Kauffmann G., Heckman T. M., Tremonti C., et al., 2003, *MNRAS*, 346, 4, 1055
 Kewley L. J., Dopita M. A., 2002, *ApJS*, 142, 1, 35
 Kewley L. J., Ellison S. L., 2008, *ApJ*, 681, 2, 1183
 Kewley L. J., Groves B., Kauffmann G., Heckman T., 2006, *MNRAS*, 372, 3, 961
 Kewley L. J., Nicholls D. C., Sutherland R. S., 2019, *ARA&A*, 57, 511
 Kobulnicky H. A., Kewley L. J., 2004, *ApJ*, 617, 1, 240
 López-Sánchez Á. R., Koribalski B. S., van Eymeren J., et al., 2012, *MNRAS*, 419, 2, 1051
 Marino R. A., Rosales-Ortega F. F., Sánchez S. F., et al., 2013, *A&A*, 559, A114
 McGaugh S. S., 1991, *ApJ*, 380, 140
 Osterbrock D. E., 1989, *Astrophysics of gaseous nebulae and active galactic nuclei*
 Pagel B. E. J., 1989, *Rev. Mexicana Astron. Astrofis.*, 18, 161
 Pedregosa F., Varoquaux G., Gramfort A., et al., 2011, *Journal of machine learning research*, 12, Oct, 2825
 Pérez-Montero E., Amorín R., 2017, *MNRAS*, 467, 2, 1287
 Pettini M., Pagel B. E. J., 2004, *MNRAS*, 348, 3, L59
 Pilyugin L. S., Thuan T. X., 2005, *ApJ*, 631, 1, 231
 Stasińska G., 2006, *A&A*, 454, 3, L127
 Teimoorinia H., Bluck A. F. L., Ellison S. L., 2016, *MNRAS*, 457, 2, 2086
 Teimoorinia H., Ellison S. L., 2014, *MNRAS*, 439, 4, 3526
 Teimoorinia H., Ellison S. L., Patton D. R., 2017, *MNRAS*, 464, 4, 3796
 Teimoorinia H., Kavelaars J. J., Gwyn S. D. J., Durand D., Rolston K., Ouellette A., 2020a, *AJ*, 159, 4, 170
 Teimoorinia H., Toyonaga R. D., Fabbro S., Bottrell C., 2020b, *PASP*, 132, 1010, 044501
 Tin Kam Ho, 1998, *IEEE Transactions on Pattern Analysis and Machine Intelligence*, 20, 8, 832
 Tremonti C. A., Heckman T. M., Kauffmann G., et al., 2004, *ApJ*, 613, 2, 898

Ucci G., Ferrara A., Pallottini A., Gallerani S., 2018, MNRAS, 477, 2, 1484
 Zaritsky D., Kennicutt Robert C. J., Huchra J. P., 1994, ApJ, 420, 87

APPENDIX A: POLYNOMIAL COEFFICIENTS FROM DR7 DATA

As shown in Fig. 1, the Kewley & Ellison (2008) polynomial coefficients derived from DR4 data are not optimized for the DR7 dataset used herein. In Tables A1 – A7 we provide updated coefficients for six of the metallicity diagnostics used in Kewley & Ellison (2008) for the DR7 dataset, using the same polynomial form, i.e.,

$$y = a + bx + cx^2 + dx^3 \quad (\text{A1})$$

y is the target calibration (i.e. what you want to convert to), and x is the metallicity that we want to convert from. The coefficients a , b , c , and d can be found for different targets. For example, suppose that we have an estimated metallicity (x) that has been obtained by method M91. If we want to convert it to (target) Z94, then we should use the coefficients in the first row of Table A2.

Furthermore, in Tables A8 – A12 we present coefficients for five more recent metallicity diagnostics included in this paper that were not available to Kewley & Ellison (2008).

Table A1. Metallicity calibration conversion constants for different inputs (x). Target (y) = **M91**

x	x-range	<i>N</i> -Galaxies	<i>a</i>	<i>b</i>	<i>c</i>	<i>d</i>
Z94	8.4 – 9.2	31443	86.793	-23.7914	2.3092	-0.0697
KD02 _(U)	8.4 – 9.2	31714	387.3987	-123.9031	13.4001	-0.4784
KD02 _(L)	8.1 – 8.4	558	600.32489	-144.5812	8.8228	0
KK04	8.25 – 9.15	32102	-2193.9176	751.0972	-85.452	3.2434
PP04 N2 _(U)	8.2 – 8.8	31133	-225.7426	79.8716	-9.1515	0.3529
PP04 N2 _(L)	8.05 – 8.3	1813	4.7727	-2.4793	0.3550	0
PP04 O3N2 _(U)	8.2 – 8.9	29042	-1033.7866	363.4906	-42.3049	1.6435
PP04 O3N2 _(L)	8.05 – 8.4	3589	-370.6417	90.1443	-5.3562	0
T04 _(U)	8.2 – 9.2	30871	-354.349	125.8661	-14.6117	0.5678
T04 _(L)	8.05 – 8.4	1160	1582.9942	-588.1495	72.992	-3.0104
M13 N2 _(U)	8.2 – 8.7	31890	98.523	-22.6664	1.425	0
M13 N2 _(L)	8.0 – 8.3	1809	-15.9858	2.9668	0	0
M13 O3N2	8.1 – 8.7	31613	91.0036	-20.7636	1.3061	0
D16 _(U)	8.0 – 9.1	30758	53.5881	-16.7644	2.0224	-0.0788
D16 _(L)	7.8 – 8.0	536	-8.4116	2.0972	0	0
C17 N2 _(U)	8.3 – 8.9	31470	95.6496	-33.318	4.092	-0.1619
C17 N2 _(L)	8.1 – 8.3	257	-3.2641	1.3817	0	0
C17 O3N2	8.25 – 8.9	32070	57.9884	-12.5818	0.7971	0

Table A2. Metallicity calibration conversion constants for different inputs (x). Target (y) = **Z94**

x	x-range	<i>N</i> -Galaxies	<i>a</i>	<i>b</i>	<i>c</i>	<i>d</i>
M91	8.4 – 9.1	31909	1825.2332	-627.9727	72.194	-2.7599
KD02	8.4 – 9.2	31680	1012.4977	-340.8346	38.446	-1.4403
KK04	8.55 – 9.2	31835	-590.5284	203.7411	-23.225	0.8876
PP04 N2	8.05 – 8.8	30912	2619.495	-924.9867	109.0873	-4.2822
PP04 O3N2	8.05 – 8.9	28917	406.0196	-140.3262	16.4181	-0.6362
T04	8.4 – 9.2	29952	830.7654	-280.1803	31.7195	-1.1925
M13 N2	8.1 – 8.7	31701	145.2596	-34.2738	2.1454	0
M13 O3N2	8.15 – 8.7	31433	1437.9466	-507.8459	59.9503	-2.3507
D16	7.9 – 9.1	30745	468.8946	-164.737	19.5684	-0.7711
C17 N2	8.2 – 8.9	31172	10.5919	-1.9581	0.2038	0
C17 O3N2	8.1 – 8.9	31701	391.6684	-124.3462	13.2068	-0.4563

Table A3. Metallicity calibration conversion constants for different inputs (x). Target (y) = **KD02**

x	x-range	<i>N</i> -Galaxies	<i>a</i>	<i>b</i>	<i>c</i>	<i>d</i>
M91 _(U)	8.5 – 9.1	31560	234.9239	-87.0053	10.8854	-0.4451
M91 _(L)	8.05 – 8.3	382	69.0297	-15.5757	0.9969	0
Z94	8.4 – 9.2	31445	-82.8695	27.6615	-2.8345	0.0993
KK04	8.2 – 9.2	32168	99.3232	-31.9684	3.6341	-0.1331
PP04 N2 _(U)	8.2 – 8.9	37304	491.9975	-178.472	21.7866	-0.8797
PP04 N2 _(L)	8.05 – 8.3	1839	335.5263	-81.3035	5.0493	0
PP04 O3N2 _(U)	8.2 – 8.9	33017	-353.9603	121.8415	-13.7148	0.5177
PP04 O3N2 _(L)	8.05 – 8.3	1420	129.8919	-30.8517	1.9554	0
T04 _(U)	8.2 – 9.2	36029	289.3069	-97.0787	11.0951	-0.4188
T04 _(L)	8.05 – 8.4	1186	-139.3008	50.8218	-5.9044	0.232
M13 N2 _(U)	8.2 – 8.7	37497	2113.0985	-744.0017	87.4392	-3.4156
M13 N2 _(L)	8.0 – 8.2	377	450.6873	-109.3972	6.7626	0
M13 O3N2	8.15 – 8.7	37214	-1831.2202	651.7518	-77.1251	3.04923
D16	8.0 – 9.1	35930	-105.37	36.6551	-3.962	0.1447
C17 N2 _(U)	8.3 – 8.9	36758	-39.973	9.7639	-0.4758	0
C17 N2 _(L)	8.1 – 8.3	258	29.1097	-5.3562	0.3433	0
C17 O3N2 _(U)	8.25 – 8.9	31992	-770.9174	271.901	-31.7625	1.2428
C17 O3N2 _(L)	8.0 – 8.25	174	-61.3755	16.8597	-1.0199	0

Table A4. Metallicity calibration conversion constants for different inputs (x). Target (y) = **KK04**

x	x-range	<i>N</i> -Galaxies	<i>a</i>	<i>b</i>	<i>c</i>	<i>d</i>
M91 _(U)	8.4 – 9.1	31919	1396.2622	-483.698	56.06155	-2.1602
M91 _(L)	8.0 – 8.25	425	721.01897	-260.4697	31.681	-1.28229
Z94	8.4 – 9.3	31894	204.83638	-69.615722	8.13631	-0.31321
KD02 _(U)	8.4 – 9.2	31689	1146.076	-388.5092	44.1343	-1.6671
KD02 _(L)	8.05 – 8.3	356	428.7191	-153.4709	18.5653	-0.74416
PP04 N2 _(U)	8.2 – 8.9	31715	1137.2633	-404.9428	48.3076	-1.9159
PP04 N2 _(L)	8.05 – 8.3	1718	221.1257	-53.9172	3.4127	0
PP04 O3N2 _(U)	8.2 – 8.9	28959	-172.8182	60.3876	-6.7529	0.2543
PP04 O3N2 _(L)	8.05 – 8.3	1343	37.2557	-8.5021	0.6094	0
T04 _(U)	8.3 – 9.2	30407	889.9372	-301.6969	34.3416	-1.2994
T04 _(L)	8.05 – 8.4	1071	3967.1747	-1449.9755	176.8893	-7.1874
M13 N2 _(U)	8.2 – 8.7	31813	3853.3363	-1367.5488	161.9577	-6.3857
M13 N2 _(L)	8.0 – 8.2	345	610.3371	-149.0526	9.2261	0
M13 O3N2	8.15 – 8.7	31550	542.1259	-193.5488	23.2532	-0.9248
D16 _(U)	8.0 – 9.1	30695	259.97912	-91.48058	11.02932	-0.44022
D16 _(L)	7.8 – 8.0	494	-1.86835	1.29895	0	0
C17 N2 _(U)	8.3 – 8.9	31385	3705.0113	-1298.9898	152.0019	-5.9222
C17 N2 _(L)	8.1 – 8.3	238	4.148	0.5126	0	0
C17 O3N2 _(U)	8.3 – 8.9	31749	-374.6472	136.3397	-16.2909	0.6538
C17 O3N2 _(L)	8.1 – 8.3	400	293.2935	-70.2175	4.3258	0

Table A5. Metallicity calibration conversion constants for different inputs (x). Target (y) = **PP04 N2**

x	x-range	<i>N</i> -Galaxies	<i>a</i>	<i>b</i>	<i>c</i>	<i>d</i>
M91 _(U)	8.5 – 9.1	31431	3613.3844	-1238.8022	141.7739	-5.4034
M91 _(L)	8.05 – 8.4	407	163.9517	-38.6531	2.398	0
Z94	8.4 – 9.3	31540	856.0385	-290.6646	33.1364	-1.2557
KD02	8.05 – 9.2	37572	865.4984	-295.5199	33.8635	-1.2895
KK04	8.2 – 9.2	32039	733.3485	-246.8248	27.9109	-1.0481
PP04 O3N2	8.05 – 8.9	38278	409.144	-143.4804	17.0264	-0.6696
T04	8.05 – 9.2	40978	524.796	-178.1117	20.3914	-0.7747
M13 N2	8.0 – 8.6	44686	163.1399	-38.4256	2.3818	0
M13 O3N2	8.1 – 8.7	43759	3794.7691	-1361.791	163.0805	-6.5026
D16	7.8 – 9.1	42591	141.2938	-49.2383	5.9996	-0.2404
C17 N2	8.0 – 8.9	43741	1229.0742	-424.8038	49.1162	-1.8864
C17 O3N2	8.0 – 8.9	44611	1196.6207	-416.474	48.5111	-1.8776

Table A6. Metallicity calibration conversion constants for different inputs (x). Target (y) = **PP04 O3N2**

x	x-range	<i>N</i> -Galaxies	<i>a</i>	<i>b</i>	<i>c</i>	<i>d</i>
M91 _(U)	8.5 – 9.1	31555	2855.1815	-976.6748	111.5376	-4.2396
M91 _(L)	8.05 – 8.4	387	-1545.1399	587.9352	-74.1884	3.1208
Z94	8.4 – 9.3	31540	342.0709	-114.2818	12.942	-0.4843
KD02	8.1 – 9.2	37672	1005.4986	-342.3498	39.0563	-1.4802
KK04	8.2 – 9.2	32100	263.38	-82.1518	8.6714	-0.2985
PP04 N2	8.05 – 8.8	42677	1733.7386	-614.419	72.766	-2.8657
T04	8.05 – 9.2	40976	425.2876	-141.5692	15.9152	-0.5918
M13 N2	8.1 – 8.7	44584	155.631	-37.0791	2.329	0
M13 O3N2	8.15 – 8.7	43840	197.388	-65.8684	7.4331	-0.2698
D16	7.8 – 9.1	42611	237.6059	-83.634	10.0731	-0.4003
C17 N2	8.1 – 8.9	43289	5361.8221	-1875.2013	218.7172	-8.4942
C17 O3N2	8.1 – 8.9	44586	-185.4252	76.7659	-10.1843	0.4513

Table A7. Metallicity calibration conversion constants for different inputs (x). Target (y) = **T04**

x	x-range	<i>N</i> -Galaxies	<i>a</i>	<i>b</i>	<i>c</i>	<i>d</i>
M91 _(U)	8.4 – 9.2	30651	2998.9561	-1030.2075	118.139	-4.5092
M91 _(L)	8.0 – 8.4	500	2.0925	0.7576	0	0
Z94	8.4 – 9.3	30155	549.9891	-185.833	21.1524	-0.7982
KD02 _(U)	8.4 – 9.3	35852	521.5475	-179.6248	20.834	-0.8003
KD02 _(L)	8.1 – 8.4	559	-2.4905	1.29317	0	0
KK04 _(U)	8.45 – 9.2	30654	1306.7925	-437.9528	49.1096	-1.8301
KK04 _(L)	8.2 – 8.4	457	-6.0523	1.7088	0	0
PP04 N2 _(U)	8.4 – 8.9	35781	-104.9897	25.3186	-1.4041	0
PP04 N2 _(L)	8.0 – 8.4	5267	-6.825	1.8446	0	0
PP04 O3N2 _(U)	8.4 – 9.2	37478	522.7574	-181.3092	21.2074	-0.8225
PP04 O3N2 _(L)	8.0 – 8.4	3600	947.9234	-349.4912	43.1432	-1.7678
M13 N2	8.0 – 8.7	40624	-804.0024	-279.9536	32.5884	-1.2538
M13 O3N2	8.1 – 8.7	39970	-1821.5398	651.9099	-77.5969	3.0867
D16 _(U)	8.1 – 9.1	39432	244.9229	-85.9962	10.3362	-0.4102
D16 _(L)	7.8 – 8.1	1608	581.3903	-188.2034	19.9897	-0.6774
C17 N2	8.2 – 8.9	39543	-43.2538	10.3962	-0.5052	0
C17 O3N2	8.2 – 8.9	40634	-1296.48795	461.04	-54.4573	2.1507

Table A8. Metallicity calibration conversion constants for different inputs (x). Target (y) = **M13 N2**

x	x-range	<i>N</i> -Galaxies	<i>a</i>	<i>b</i>	<i>c</i>	<i>d</i>
M91 _(U)	8.5 – 9.1	31560	1559.59	-537.0831	61.9093	-2.3757
M91 _(L)	7.9 – 8.4	562	48.3787	-10.4483	0.6772	0
Z94	8.4 – 9.3	31669	226.7235	-77.9489	9.2069	-0.3599
KD02 _(U)	8.4 – 9.3	37326	380.7872	-131.0384	15.2996	-0.5928
KD02 _(L)	8.2 – 8.4	528	-0.7239	1.6589	-0.0704	0
KK04 _(U)	8.55 – 9.2	31612	805.682	-273.9803	31.3139	-1.1903
KK04 _(L)	8.2 – 8.4	447	4.352	0.4586	0	0
PP04 N2	8.0 – 8.9	44709	-460.0623	158.8308	-17.9864	0.6805
PP04 O3N2	8.0 – 9.2	44585	-86.985	28.6534	-2.8417	0.093
T04 _(U)	8.55 – 9.2	38918	0.3458	-1.8454	0.6829	-0.0418
T04 _(L)	8.0 – 8.5	2020	574.6886	-212.1147	26.3888	-1.0909
M13 O3N2	8.1 – 8.7	44085	120.9708	-52.0238	7.5124	-0.3468
D16	7.8 – 9.1	42863	-64.0936	22.8361	-2.3987	0.0842
C17 N2	8.0 – 8.9	43734	932.1046	-329.5358	39.0721	-1.5398
C17 O3N2	8.0 – 8.9	44929	697.0506	-247.6338	29.572	-1.1729

Table A9. Metallicity calibration conversion constants for different inputs (x). Target (y) = **M13 O3N2**

x	x-range	<i>N</i> -Galaxies	<i>a</i>	<i>b</i>	<i>c</i>	<i>d</i>
M91 _(U)	8.5 – 9.1	31282	1888.2496	-644.077	73.4676	-2.7899
M91 _(L)	8.0 – 8.3	167	-1305.8981	491.485	-61.2792	2.547
Z94	8.4 – 9.3	31417	341.7221	-113.7254	12.8692	-0.483
KD02	8.4 – 9.3	37043	967.8764	-328.278	37.3634	-1.4146
KK04 _(U)	8.55 – 9.2	31362	536.8013	-176.7522	19.6262	-0.7232
KK04 _(L)	8.2 – 8.4	116	98.1808	-21.7183	1.3102	0
PP04 N2	8.2 – 8.9	43757	1204.6286	-425.8859	50.4443	-1.9879
PP04 O3N2	8.2 – 9.1	43707	234.8163	-81.3845	9.6777	-0.3809
T04 _(U)	8.55 – 9.2	38815	182.9739	-61.21	7.0837	-0.2707
T04 _(L)	8.1 – 8.5	1477	2411.7063	-867.0572	104.2289	-4.175
M13 N2	8.2 – 8.65	44082	6083.3786	-2158.8367	255.5638	-10.0782
D16	7.8 – 9.1	42012	214.9474	-74.7581	8.962	-0.3559
C17 N2	8.3 – 8.9	42782	5320.2935	-1857.9627	216.4846	-8.4027
C17 O3N2	8.3 – 8.9	44083	0.3628	0.9335	0	0

Table A10. Metallicity calibration conversion constants for different inputs (x). Target (y) = **D16**

x	x-range	<i>N</i> -Galaxies	<i>a</i>	<i>b</i>	<i>c</i>	<i>d</i>
M91 _(U)	8.5 – 9.1	30613	2541.5169	-873.1917	100.1378	-3.8204
M91 _(L)	8.0 – 8.3	471	5.1048	0.3513	0	0
Z94	8.4 – 9.3	30224	3706.8072	-237.5519	26.8035	-1.0031
KD02 _(U)	8.4 – 9.3	35949	1292.1462	-439.7038	50.0465	-1.8928
KD02 _(L)	8.2 – 8.4	524	3.3878	0.5506	0	0
KK04 _(U)	8.55 – 9.2	30663	875.0474	-289.4371	32.0548	-1.1768
KK04 _(L)	8.2 – 8.4	443	2.8759	0.6069	0	0
PP04 N2	8.1 – 8.9	41901	957.6926	-337.1474	39.7259	-1.5529
PP04 O3N2	8.0 – 9.2	41944	284.8894	-99.0825	11.6981	-0.4551
T04 _(U)	8.5 – 9.3	39034	-252.7935	87.9578	-10.0078	0.3848
T04 _(L)	8.0 – 8.5	2015	1028.8981	-371.8225	45.0596	-1.8169
M13 N2	8.0 – 8.7	42210	-1633.1334	615.017	-76.9143	3.2096
M13 O3N2	8.15 – 8.65	41348	-718.1404	264.3618	-32.295	1.3239
C17 N2	8.0 – 8.9	41006	2375.3459	-823.6716	95.2887	-3.6646
C17 O3N2	8.0 – 8.9	42175	-482.1501	183.9562	-23.1037	0.9705

Table A11. Metallicity calibration conversion constants for different inputs (x). Target (y) = **C17 N2**

x	x-range	<i>N</i> -Galaxies	<i>a</i>	<i>b</i>	<i>c</i>	<i>d</i>
M91 _(U)	8.4 – 9.1	31170	2901.7049	-994.8047	113.9298	-4.3457
M91 _(L)	8.0 – 8.4	502	2.5221	0.7141	0	0
Z94	8.4 – 9.3	30636	383.5379	-130.358	15.0295	-0.5747
KD02 _(U)	8.4 – 9.2	36412	642.9785	-220.0287	25.3594	-0.9713
KD02 _(L)	8.2 – 8.4	531	-4249.5242	1535.7596	-184.7107	7.4079
KK04 _(U)	8.55 – 9.2	31083	986.5064	-334.2708	38.0059	-1.4373
KK04 _(L)	8.2 – 8.4	452	3.0422	0.6294	0	0
PP04 N2	8.0 – 8.9	43044	-1175.2954	413.3419	-48.1757	1.8745
PP04 O3N2	8.0 – 9.2	42596	-7.9268	1.0615	0.3627	-0.0305
T04 _(U)	8.55 – 9.2	37884	371.1892	-127.1447	14.7861	-0.5704
T04 _(L)	8.0 – 8.5	2024	230.5072	-90.1699	11.9911	-0.5242
M13 N2	8.0 – 8.6	43036	-2591.8417	935.0384	-112.197	4.4924
M13 O3N2	8.15 – 8.65	42099	1256.816	-457.1278	55.6542	-2.2528
D16	7.8 – 9.1	40982	-83.8363	30.1166	-3.295	0.1213
C17 O3N2	8.0 – 8.9	42941	445.5391	-158.2197	18.9688	-0.7533

Table A12. Metallicity calibration conversion constants for different inputs (x). Target (y) = **C17 O3N2**

x	x-range	<i>N</i> -Galaxies	<i>a</i>	<i>b</i>	<i>c</i>	<i>d</i>
M91 _(U)	8.5 – 9.1	31560	1922.6664	-659.1048	75.5519	-2.8829
M91 _(L)	8.0 – 8.3	477	-31.2375	9.0558	-0.5155	0
Z94	8.4 – 9.3	31669	73.9083	-25.0406	3.0904	-0.1237
KD02 _(U)	8.4 – 9.2	37208	719.4539	-245.8567	28.2585	-1.0795
KD02 _(L)	8.1 – 8.4	559	-100.2682	25.5497	-1.5024	0
KK04	8.2 – 9.2	32168	302.3792	-100.4709	11.3665	-0.4254
PP04 N2	8.05 – 8.9	44599	302.2795	-112.1483	14.0962	-0.5843
PP04 O3N2	8.05 – 9.2	44583	7.1195	-4.0341	0.9299	-0.0512
T04 _(U)	8.55 – 9.2	38918	-86.437	28.1687	-2.7891	0.0926
T04 _(L)	8.0 – 8.5	2025	431.9057	-164.2151	21.06348	-0.8947
M13 N2	8.0 – 8.65	44930	1479.4498	-528.8548	63.2182	-2.5125
M13 O3N2	8.1 – 8.7	44083	-464.0953	161.6573	-18.517	0.7109
D16	7.8 – 9.1	42829	29.5937	-10.6313	1.5776	-0.0725
C17 N2	8.0 – 8.9	43636	1860.3708	-657.1819	77.5899	-3.0477